HHS Public Access

Author manuscript

Nat Immunol. Author manuscript; available in PMC 2014 August 01.

Published in final edited form as:

Nat Immunol. 2014 February ; 15(2): 186–194. doi:10.1038/ni.2772.

Inhibition of Csk in thymocytes reveals a requirement for actin remodeling in the initiation of full T cell receptor signaling

Ying Xim Tan[1], **Boryana N. Manz**[1], **Tanya Freedman**[1], **Chao Zhang**[3], **Kevan M. Shokat**[4,5], and **Arthur Weiss**[1,2,5]

[1]Rosalind Russell Medical Research Center for Arthritis, Division of Rheumatology, Department of Medicine, University of California, San Francisco, CA 94143, USA

[2]Department of Microbiology and Immunology, University of California, San Francisco, CA 94143, USA

[3]Department of Chemistry, University of Southern California, CA 90089, USA

[4]Department of Cellular and Molecular Pharmacology, University of California, San Francisco, CA 94143, USA

[5]Howard Hughes Medical Institute, Chevy Chase, MD 20815

Abstract

T cell receptor (TCR) signaling is initiated by Src-family kinases (SFKs). To understand how C-terminal Src kinase (Csk), the negative regulator of SFKs, controls the basal state and the initiation of TCR signaling, we generated mice expressing a PP1-analog inhibitor-sensitive Csk variant (Csk^{AS}). Inhibition of Csk^{AS} in thymocytes, without TCR engagement, induced potent SFK activation and proximal TCR signaling up to phospholipase C-γ1 (PLC-γ1). Surprisingly, increases in inositol phosphates (InsP), intracellular calcium and Erk phosphorylation were impaired. Altering the actin cytoskeleton pharmacologically or providing CD28 costimulation rescued these defects. Thus, Csk plays a critical role in preventing TCR signaling. However, our studies also revealed a requirement for actin remodeling, initiated by costimulation, for full TCR signaling.

Signals transduced by the TCR are critical for thymocyte selection and maturation, peripheral T cell homeostasis and activation, as well as specification of effector and memory cell fates. Hence the initiation of TCR signaling in response to antigens of diverse affinities at different stages of T cell development must be tightly regulated. This regulation ensures the selection of a protective T cell repertoire and the mounting of efficacious immune responses against foreign pathogens while preventing aberrant immune activation. The TCR complex has no intrinsic kinase activity but instead possesses two spatially separated

Author Contributions

Y.X.T. and A.W. designed the research and wrote the manuscript, Y.X.T. performed the research and analyzed the data. B.N.M. helped design, perform and analyze the immunofluorescence experiments. T.F. designed, performed and analyzed the data from the *in vitro* kinase assays. C.Z. and K.M.S. designed the Csk^{AS} allele and provided 3-IB-PP1. All authors commented on the manuscript.

tyrosines within immunoreceptor tyrosine-based activation motifs (ITAMs) located in the cytoplasmic tails of its non-ligand binding CD3 and ζ subunits[1]. Phosphorylation of these ITAMs is mediated by the T cell SFKs Lck and Fyn T, thereby creating docking sites for the recruitment of the cytoplasmic kinase ZAP-70 via its tandem SH2 domains. The autoinhibited conformation of ZAP-70 is relieved by ITAM binding as well as by its phosphorylation by Lck or Fyn T. ZAP-70 activation is critical for downstream signaling events leading to cellular responses.

In freshly isolated resting thymocytes and T cells, non-phosphorylated ZAP-70 is bound to constitutively phosphorylated ITAMs[2]. Following prolonged cell culture, the constitutively phosphorylated state of the ITAMs in primary cells is lost but is reinduced by TCR stimulation, as it is in T cell lines. Various mechanisms have been proposed for how ITAM and/or ZAP-70 phosphorylation by SFKs is initiated during TCR stimulation. These include co-ligation of the CD4 or CD8 coreceptors with the TCR by peptide-bound major histocompatibility complex (pMHC), which redistributes the coreceptor-associated SFK Lck into proximity with TCR ITAMs–ZAP-70; TCR conformational change induced by pMHC binding that permits increased ITAM accessibility to SFKs; and redistribution of bulky transmembrane phosphatases that inhibit signaling away from the narrow TCR-pMHC cell-cell interface due to size exclusion (i.e. kinetic segregation model)[3–5]. The relative importance of these mechanisms is unresolved because the experimental evidence available is conflicting or incomplete. It is also uncertain if any of these mechanisms alone is sufficient to trigger full TCR downstream signaling.

Since SFKs phosphorylate TCR ITAMs, the control of their activities represents a key regulatory node in the initiation of TCR signaling. Trans-autophosphorylation of a conserved activation loop tyrosine within the SFK catalytic domain increases catalytic activity[6]. Phosphorylation of the conserved C-terminal inhibitory tyrosine of SFKs by the tyrosine kinase Csk promotes their closed, inactive conformation[7]. In T cells, the receptor-like tyrosine phosphatase CD45 opposes the action of Csk and dephosphorylates the inhibitory tyrosine. Thus, the equilibrium between Csk and CD45 may set the threshold for activation of TCR signaling[8]. In resting T cells, there are multiple phosphorylation states of Lck, which consists of unphosphorylated, each of the singly phosphorylated and the doubly phosphorylated species[9]. It is unclear if this basal equilibrium has a fixed state or is a dynamic, ongoing process in unstimulated primary T cells.

Ubiquitously expressed, Csk is a cytosolic protein. Since Csk-deficient mice are embryonic lethal due to excessive SFK activity and conditional deletion of Csk in thymocytes results in TCR- and MHC-independent development of abnormal $CD4^+$ T cells, understanding the importance of Csk regulation in the T cell lineage has been challenging[10–12]. Positioning Csk at the plasma membrane, proximal to the membrane-localized SFKs, is thought to be regulated through protein-protein interactions that may mediate its dynamic translocation between the cytosol and the cell membrane[13]. The lipid raft-localized adaptor phosphoprotein associated with glycosphinogolipid-enriched microdomains (PAG) is believed to be involved in the recruitment of Csk to lipid rafts where some SFK molecules are localized and initiation of TCR signaling may occur[14–17]. However, in sharp contrast to

Csk deficiency, PAG-deficient mice develop normally without defect in T cell development or signaling, indicating the existence of alternative mechanisms for Csk regulation[18, 19].

To interrogate the role of Csk activity in TCR signaling, we recently generated a novel allele of *Csk* (Csk^{AS}) by mutating the conserved bulky gatekeeper residue in its ATP-binding pocket, thereby enlarging the pocket. Csk^{AS} kinase activity is specifically and rapidly inhibited by 3-iodo-benzyl-PP1 (3-IB-PP1), a bulky analog of the common kinase inhibitor, PP1. Unexpectedly, in Jurkat T cells, inhibiting the kinase activity of a dominant inhibitory membrane-targeted Csk^{AS} induced potent SFK activation and ligand-independent TCR signaling[20]. This finding suggests that perturbing the finely tuned Csk-CD45 kinase-phosphatase activity equilibrium can lead to SFK activation and trigger TCR signal initiation. However, Jurkat T cells express endogenous Csk; so, the expression of membrane-targeted Csk^{AS} may have induced compensatory rewiring of the signaling circuitry or activation could have reflected a dominant-negative effect mediated by the protein interaction domains of the inhibited Csk^{AS}.

To determine the role of Csk in controlling the basal state and TCR signal initiation in primary T lineage cells, we generated mice expressing only the normally regulated cytosolic form of Csk^{AS}. We found that inhibition of Csk^{AS} alone in thymocytes led to strong activation of SFKs and proximal signaling, but did not result in full downstream TCR signaling in the absence of additional actin cytoskeletal remodeling. Our data suggests that Csk plays a major role in restraining SFK activation in the basal state and that SFK activation alone is sufficient for the initiation of proximal TCR signaling. However, our studies also indicate that in addition to SFK activity, the actin cytoskeleton must be remodeled in thymocytes for downstream signal propagation. This required cytoskeletal remodeling is most likely mediated by CD28 costimulation.

Results

Generation of Csk^{AS} mice

We introduced Csk^{AS} into mice by bacterial artificial chromosome (BAC) transgenesis. The Csk^{AS} allele is 25% as active as wild-type Csk (Supplementary Fig. 1a, b). We obtained three independent founders and crossed them with $Csk^{+/-}$ mice, ultimately removing expression of endogenous wild-type Csk. Two of the lines expressed less than 50% Csk as compared to wild-type mice and displayed defects in T cell development (data not shown). The third line had approximately 2.5-fold as much expression of Csk as wild-type mice, but displayed normal T cell development (Supplementary Fig. 2a–c). Importantly, Csk^{AS} thymocytes had TCR responses to stimulation with both high and low doses of anti-CD3 mAb comparable to wild-type (Supplementary Fig. 2d). We therefore conducted further studies with this third Csk^{AS} transgenic line.

Inhibiting Csk^{AS} activates SFKs and proximal TCR signals

At 10 μM, 3-IB-PP1 strongly inhibited recombinant Csk^{AS} but not wild-type Csk (Supplementary Fig. 1c,d). Treatment of thymocytes or peripheral $CD4^+$ T cells with 3-IB-PP1 rapidly led to sustained hyperphosphorylation of the activation loop tyrosine of both

Lck and Fyn, as well as slower progressive dephosphorylation of the inhibitory tyrosine of Lck, in Csk^{AS} but not wild-type cells (Fig. 1a,b). Those data reaffirm the role of Csk as the primary negative regulator of SFKs. The findings also indicate that in mouse T cells, the basal phosphorylation status of Lck is in a dynamic equilibrium that requires constant restraint by Csk activity. Removal of this constraint drives rapid ligand-independent autoactivation of SFKs, presumably by trans-autophosphorylation. The incomplete dephosphorylation of the inhibitory tyrosine of Lck may imply that a subset of Lck molecules is shielded from or is inaccessible to CD45 phosphatase activity.

The activation of Lck could lead to TCR signaling initiation. Lck phosphorylates TCR CD3 and ζ-chain ITAMs, allowing for the recruitment, phosphorylation and activation of ZAP-70. Active ZAP-70 phosphorylates LAT and SLP-76, which form a supramolecular signalosome that recruits PLC-γ1. Subsequent phosphorylation of PLC-γ1 on tyrosine 783 by Tec family kinases leads to its activation and the hydrolysis of phosphatidylinositol 4,5-bisphosphate ($PtdIns(4,5)P_2$)[1]. The Class I Phosphoinositide-3-kinase-δ (PI(3)K-δ) is also activated upon TCR stimulation, and phosphorylates $PtdIns(4,5)P_2$ to phosphatidylinositol 3,4,5-trisphosphate ($PtdIns(3,4,5)P_3$) that regulates Akt phosphorylation[21]. In thymocytes, Lck activation in response to Csk^{AS} inhibition led to increased global tyrosine phosphorylation, including CD3ζ-p23 phosphorylation (Fig. 1c,d and Supplementary Fig. 3a). Csk^{AS} inhibition also induced phosphorylation of ZAP-70, LAT, PLC-γ1 and Akt in thymocytes, comparably to that resulting from CD3 crosslinking (Fig. 1e and Supplementary Fig. 3b). The phosphorylation of both PLC-γ1 and Akt is consistent with Tec kinase activation in response to Csk inhibition. Overall, our data implies that inhibiting Csk increases activation of SFKs, leading to the proximal phosphorylation events associated with TCR signaling even without receptor engagement. In contrast to the conformational change and kinetic segregation models of TCR triggering, our findings suggest that by activating SFKs, proximal signaling can be initiated even without inducing TCR conformational change or segregating the TCR from abundant large transmembrane phosphatases such as CD45.

Impaired Ca^{2+} and Ras-Erk signals upon Csk^{AS} inhibition

Active PLC-γ1 hydrolyses $PtdIns(4,5)P_2$ into diacylglycerol (DAG) and inositol 1,4,5-trisphosphate ($Ins(1,4,5)P_3$) that activate the Ras-Erk and the calcium (Ca^{2+}) signaling pathways, respectively[1]. Surprisingly, in contrast to TCR stimulation with anti-CD3, the inhibition of Csk^{AS} that led to similar increases in PLC-γ1 phosphorylation in thymocytes was not associated with robust Erk phosphorylation or increased intracellular calcium (Fig. 2a,b). The low-level Erk phosphorylation seen in DP thymocytes was not sufficient to drive CD69 upregulation (Supplementary Fig. 3c). The defect in Erk phosphorylation was more severe in peripheral $CD4^+$ T cells, and this correlated with reduced ZAP-70, LAT and PLC-γ1 phosphory lation relative to CD3 crosslinking (Fig. 2a,b and Supplementary Fig. 3d,e).

$Ins(1,4,5)P_3$ is rapidly metabolized to inositol 1,4-bisphosphate ($Ins(1,4)P_2$) and inositol 1-phosphate ($Ins(1)P_1$)[22]. Therefore, measuring total InsP production in the presence of lithium chloride, an inhibitor of $Ins(1)P_1$ phosphatase, reflects overall hydrolysis of $PtdIns(4,5)P_2$ by PLC-γ1. We found that total InsP production in thymocytes was severely

impaired following Csk^{AS} inhibition relative to TCR stimulation (Fig. 3a). The small increase in total InsP implies a corresponding low amount of DAG that may be sufficient to activate the Ras guanine exchange factor (RasGEF) RasGRP1 but may not generate enough Ras-GTP to drive the positive feedback loop for Ras activation by SOS, a RasGEF that is allosterically activated by Ras-GTP. This may account for the very low amounts of Erk phosphorylation we observed. Alternatively, the recently described PLC-γ1-independent RasGRP1-Erk pathway may be involved[23].

Actin cytoskeleton alteration restores full TCR signals

The cortical actin cytoskeleton restricts lateral diffusion of transmembrane molecules[24], and actin-binding proteins can sequester $PtdIns(4,5)P_2$ (refs. 25, 26). Altering the actin cytoskeleton alone in primary B cells can activate calcium and Erk pathways[27]. We speculated that the cortical actin cytoskeleton might limit the PLC-γ1 activity induced downstream of Csk^{AS} inhibition. Indeed, Csk^{AS} thymocytes treated simultaneously with 3-IB-PP1 and the actin-modifying agent, cytochalasin D, had increased total IP, intracellular calcium and Erk phosphorylation that was comparable to that seen with CD3 crosslinking (Fig. 3a–c). In contrast, treatment of Csk^{AS} thymocytes with cytochalasin D alone did not result in an increase in intracellular calcium or Erk phosphorylation. Similar responses were observed with other actin-modifying agents (Supplementary Fig. 4). The striking increase in $PtdIns(4,5)P_2$ hydrolysis and downstream responses induced by altering the actin cytoskeleton was not accounted for by changes in PLC-γ1 phosphorylation (Fig. 3d). These data suggest that actin cytoskeletal remodeling plays a crucial role in downstream TCR signaling events in thymocytes by controlling the access of PLC-γ1 to $PtdIns(4,5)P_2$. In contrast, Akt phosphorylation was induced by Csk^{AS} inhibition alone, indicating that PI(3)K access to $PtdIns(4,5)P_2$ and Akt access to $PtdIns(3,4,5)P_3$ were not as strongly regulated by the actin cytoskeleton.

Altering the actin cytoskeleton in peripheral $CD4^+$ T cells, however, only partially restored the defect in intracellular calcium increase and Erk phosphorylation following Csk^{AS} inhibition (Fig. 3e,f). Combined with our earlier observation that proximal phosphorylation induced by Csk^{AS} inhibition in peripheral $CD4^+$ T cells was impaired (Supplementary Fig. 3e), it appears that additional regulatory mechanisms for signal initiation develop in more mature T cells. In support of this possibility, we found that although Csk^{AS} inhibition alone induced strong Erk phosphorylation in immature thymic γδ T cells, this responsiveness was greatly reduced in mature splenic γδ T cells, which behaved similarly to peripheral $CD4^+$ T cells (Fig. 3g,h). Thus, altering the actin cytoskeleton rescues the defect in calcium and Ras-Erk signaling following Csk^{AS} inhibition in immature thymocytes but not in mature peripheral T cells.

Mature dendritic cells restore full TCR signaling

We sought to determine if there is a physiologic costimulus that could induce the requisite cytoskeletal remodeling in thymocytes that was not achieved in response to SFK activation by Csk^{AS} inhibition alone. *In vivo*, thymocytes initiate TCR signaling when they recognize pMHC molecules on antigen-presenting cells (APCs) such as thymic epithelial cells or dendritic cells (DCs). APCs also express numerous costimulatory molecules that can

provide additional signals. The TCR signal together with costimulatory signals dictate thymocyte developmental fate[28]. Remarkably, interaction of the polyclonal thymocytes with activated but not naïve splenic DCs, in thymocyte-DC conjugates, enhanced Erk phosphorylation and increased intracellular calcium in Csk^{AS} thymocytes when Csk^{AS} was inhibited (Fig. 4a,b and Supplementary Fig. 5a). Since *in vitro* activated splenic DCs may differ from thymic DCs[29], the physiologic APCs for thymocytes, we tested the ability of thymic DCs to enhance Erk phosphorylation induced by Csk^{AS} inhibition. Thymic DCs did enhance Erk activation in 3-IB-PP1-treated Csk^{AS} cells, albeit to a lesser extent than mature splenic DCs (Supplementary Fig. 5b). Overall, our findings demonstrate that mature DCs can restore full TCR signaling following Csk^{AS} inhibiton.

DCs need CD80, CD86 and MHC to restore full TCR signals

We postulated that DCs restore full activation of TCR signaling leading to calcium increase and Erk activation in response to Csk^{AS} inhibition by providing a costimulatory signal that initiated cytoskeletal remodeling. Using a candidate approach, we tested the role of several pathways known to influence actin remodeling during T cell-APC interactions[30]. The diminished ability of activated CD80-CD86 doubly deficient DCs to enhance 3-IB-PP1-induced Erk phosphorylation implicated the importance of their receptor CD28 (Fig. 5a). In contrast, activated intercellular adhesion molecule-1 (ICAM-1)-deficient DCs enhanced 3-IB-PP1-induced Erk phosphorylation as potently as wild-type DCs, suggesting the T cell integrin lymphocyte function-associated antigen 1 (LFA-1) was dispensable (Supplementary Fig. 5c). Likewise, inhibition of G_i-protein coupled receptor signaling in thymocytes by using pertussis toxin had no effect, arguing against the involvement of chemokine receptors (Supplementary Fig. 5d). Most Lck in thymocytes is associated with CD4 or docking with MHC, they recruit coreceptor-bound Lck to the TCR[31]. We found that MHCI and MHCII doubly deficient activated DCs had diminished ability to enhance Erk phosphorylation upon 3-IB-PP1 treatment (Fig. 5b). Similarly, we observed that activated CD80-CD86 doubly deficient or MHCI and MHCII doubly deficient DCs had reduced ability to induce intracellular calcium increase in Csk^{AS} thymocytes treated with 3-IB-PP1 (Fig. 5c,d). Thus, our data reveal that activated DCs require expression of CD28 counter-ligands and MHC to restore full TCR signaling in thymocytes leading to calcium and Erk responses when Csk^{AS} is inhibited. This finding is consistent with our observation that naïve DCs could not restore full TCR signaling (Supplementary Fig. 5a), since CD80, CD86 and MHC molecules are upregulated during DC maturation[32].

CD28 engagement restores robust ERK phosphorylation

We next examined whether providing the CD28-CD86 interaction alone is sufficient to enhance Erk phosphorylation following Csk^{AS} inhibition. Indeed, inhibition of Csk^{AS} in thymocytes in the presence of CD86-Ig coated beads increased Erk phosphorylation. Moreover, coating the beads with both CD86-Ig and class II MHC tetramer further increased the extent of Erk phosphorylation, even though class II MHC tetramer alone did not increase Erk phosphorylation (Fig 6a). This result provides evidence that CD28-CD86–induced signals are sufficient to restore robust Erk signaling following Csk^{AS} inhibition, particularly when MHC-mediated interactions are also present.

CD28 engagement induces actin remodeling

We hypothesized that the CD28-mediated costimulation provided by activated DCs restored robust Erk activation by inducing actin remodeling in thymocytes. CD28 signaling has been shown to induce both PI(3)K activation and actin remodeling[33, 34]. The YMNM motif in its cytoplasmic tail recruits the p85 subunit of PI(3)K. In addition, the actin cytoskeletal regulators Vav-1, cofilin-1 and Rltpr are activated downstream of CD28 (ref. 35). To determine if PI(3)K signaling plays a role in the restoration of full TCR signaling by activated DCs, we pre-treated thymocytes with the PI(3)K inhibitor LY294002 before Csk^{AS} inhibition in the presence of activated DCs. We found that although Akt phosphorylation was completely abrogated as expected, the enhancement in Erk phosphorylation was unaffected, suggesting that PI(3)K signaling is not important for this effect (Fig. 6b).

We then explored the role of CD28 signaling in actin remodeling by imaging the F-actin distribution of thymocytes conjugated to CD86-Ig coated beads and treated with 3-IB-PP1. We observed F-actin polarization and accumulation at the thymocytes-CD86-Ig bead interface when Csk^{AS} was inhibited (Fig. 6c, d). In contrast, 3-IB-PP1 alone induced only a negligible amount of F-actin polarization, indicating that this actin remodeling required both CD28 engagement and SFK activation. In conclusion, our data supports the following model. Upon SFK activation, actin remodeling, which can be induced by CD28 engagement, allows for the hydrolysis of PtdIns(4,5)P_2 by active PLC-γ1, resulting in the downstream propagation of full TCR signals in thymocytes (Supplementary Fig. 6).

Discussion

In this study, we have generated mice expressing Csk^{AS}, allowing for genetically specific and rapid inhibition of Csk kinase activity in cells. This has enabled us to elucidate for the first time, the function of Csk kinase activity in the initiation of TCR signaling in unmanipulated primary T cells. Following Csk^{AS} inhibition in thymocytes, we observed rapid hyperactivation of Lck and Fyn T, which in turn induced the phosphorylation of proximal TCR signaling components up to and including PLC-γ1. We propose that a dynamic equilibrium of Csk and CD45 activity controls SFK activity, and is responsible for maintaining the basal unstimulated state of the most proximal components of the TCR signaling pathway. Such an ongoing equilibrium may confer rapid plasticity of Lck activation status, allowing for sensitive and efficient TCR triggering in response to receptor engagement. Our results also suggest that Csk plays the dominant inhibitory role in controlling the basal state and may largely be responsible for setting the threshold for TCR signaling. Inhibition of Csk function without CD45 perturbation or induction of TCR-CD3 conformational change can therefore play a prominent physiologic role in allowing SFKs to be activated and initiate downstream TCR-dependent signaling. Physiologically, local changes induced by ligating the TCR can be envisioned to influence this equilibrium through various mechanisms that might influence Csk, CD45 or Lck (or Fyn T) localization. ITAM accessibility seems to be less of a concern since the CD3 ζ chain is already largely constitutively phosphorylated *in vivo* in the basal state, albeit there is a modest increase in its phosphorylation following receptor stimulation.

Notably, our results also suggest that activation of SFK activity alone is insufficient to initiate the full downstream signaling pathway leading to calcium and Erk responses, events critical for cellular activation. In thymocytes, downstream pathway activation requires events that lead to actin cytoskeletal remodeling to allow PLC-γ1 access to PtdIns(4,5)P_2. Thus, the actin cytoskeleton can provide a barrier to control the transmission of downstream signaling events. The required actin remodeling to overcome this barrier may be accomplished experimentally *ex vivo* by ligation of TCR with very high concentrations of mAbs and pMHC complexes. Under physiologic conditions where TCR stimuli is limiting, the function of other coreceptors or costimulatory molecules, such as CD28, that influence actin cytoskeletal remodeling, is likely necessary for PLC-γ1 to access its substrate.

The requirement for actin remodeling in primary thymocytes to initiate full TCR signaling is in contrast to our previous findings in Jurkat T cells[20]. Inhibiting Csk in Jurkat T cells, in the absence of TCR engagement and additional actin cytoskeletal manipulation, resulted in substantial intracellular calcium increases, Erk phosphorylation and the upregulation of CD69. One reason may be that the cortical actin cytoskeletal dynamics of Jurkat T cells and primary T cells are different. Jurkat T cells lack expression of PTEN and SHIP-1 phosphatases that dephosphorylate PtdIns(3,4,5)P_3, and most likely have an abnormal phosphoinositide composition in their plasma membrane[36]. This could in turn have a profound impact on their cortical actin cytoskeleton, since PtdIns(4,5)P_2 and PtdIns(3,4,5)P_3 regulate F-actin assembly in cells by binding and influencing the activity of numerous actin regulatory proteins[37].

Another notable difference we observed in response to Csk inhibition was between thymocytes and mature $CD4^+$ T cells. Similar to thymocytes, mature $CD4^+$ T cells displayed strong SFK activation after 3-IB-PP1 treatment, but in contrast to thymocytes, the phosphorylation of ZAP-70, LAT and PLC-γ1 was reduced compared to anti-CD3 crosslinking. Furthermore, altering the actin cytoskeleton in mature $CD4^+$ T cells only partially restored the calcium and MAPK signaling following Csk^{AS} inhibition. We observed similar differences in the response to Csk^{AS} inhibition between immature thymic γδ T cells and mature splenic γδ T cells. There are likely additional negative regulatory pathways, acquired during development, perhaps involving phosphatases or inhibitory receptors, which have to be overcome in mature T cells. Alternatively, mature T cells may have different regulatory mechanisms governing their cortical actin cytoskeletons. Interestingly, thymic γδ T cells were able to phosphorylate Erk robustly without the need for additional actin remodeling stimulus following Csk^{AS} inhibition, further underscoring the fact that different T cell subsets have distinct regulation of their signal transduction pathway, most likely due to differences in the wiring of their signaling networks.

Actin cytoskeletal dynamics play multiple important roles in T cell activation and have been best studied in the context of the immunological synapse (IS), a supramolecular structure found at the contact site between a T cell and an APC, and is proposed to be important for prolonging and modulating TCR signaling. F-actin first accumulates in the T cell-APC interface and is then followed by a central clearing. Disruption of the actin cytoskeleton with cytochalasin D impairs formation of TCR microclusters and the IS[30]. Numerous pathways downstream of TCR or costimulation that are involved in actin remodeling and important for

IS formation have been identified. On the other hand, exactly how actin dynamics influence TCR signaling remains elusive. Stimulating cytochalasin D treated T cells with superantigen-pulsed APCs leads to reduced calcium flux but stimulating the same T cells with anti-CD3 leads to prolonged calcium flux[38]. Our results clearly reveal a previously unappreciated direct role for actin cytoskeletal dynamics in the initiation of calcium and MAPK signaling in thymocytes.

A recent report demonstrated that merely altering the actin cytoskeleton in primary naïve B cells results in a spontaneous increase in intracellular calcium that is dependent on antigen receptor signaling[27]. In contrast, in primary thymocytes, we have shown that altering the actin cytoskeleton alone did not initiate any TCR signaling events and that additional activation of SFKs was required for full TCR signaling. This difference between T and B cells may reflect their differing dependence on basal signaling for peripheral homeostasis and suggests that initiation of TCR signaling is more tightly regulated[39, 40]. The hypothesis proposed suggests that in B cells, actin cytoskeletal remodeling allows for greater BCR mobility and increases its interactions with downstream signaling molecules such as CD19 (ref. 27). A similar finding is unlikely to be the case in thymocytes, since SFK activation alone was sufficient to induce proximal phosphorylation events. In thymocytes, it appears that the predominant role of the cortical actin cytoskeleton is in regulating PLC-γ1 access to PtdIns(4,5)P_2.

Lending physiologic significance to our finding that actin cytoskeletal remodeling was required for full TCR signaling was our observation that activated DCs could restore calcium and Ras-ERK signaling upon Csk^{AS} inhibition in thymocytes. This required the presence of CD80 or CD86 costimulatory molecules on the DCs. Indeed, providing CD28 costimulation alone during Csk^{AS} inhibition was sufficient to enhance Erk phosphorylation. CD28 signaling induces pathways including PI(3)K activation and actin cytoskeletal remodeling[33]. Our results demonstrate that the CD28-dependent rescue of Ras-Erk signaling does not require PI(3)K activation. Moreover, we show that CD28 signaling induces actin remodeling and polarization of the cortical actin cytoskeleton in thymocytes upon Csk^{AS} inhibition. Whether the function of CD28 costimulation is to provide a qualitatively different input to complement TCR signals or serves to quantitatively enhance TCR signal strength has remained an open question. Our data provides evidence supporting the idea that CD28 costimulation delivers a unique actin cytoskeletal remodeling signal that is required for the initiation of complete TCR signaling in thymocytes. Surface expression of CD28 is highest on thymocytes, however, the role of CD28 in thymic positive and negative selection remains contentious[41–43]. We also cannot fully exclude the possibility that other costimulatory molecules interacting with ligands on thymic epithelial cells or other cells resident in the thymus provide actin remodeling signals similar to those provided by CD28.

Finally, we propose the following model for TCR signal propagation in thymocytes: When a thymocyte encounters an APC bearing its cognate pMHC, active Lck initiates a tyrosine phosphorylation cascade that leads to the phosphorylation and activation of PLC-γ1. Simultaneously, because Lck interacts with and phosphorylates CD28 (ref. 44), the costimulatory CD28-CD80 (or CD28-CD86) interaction delivers local actin remodeling signals at the site of active TCR signaling. This enables LAT-bound PLC-γ1 to come into

sufficient proximity to PtdIns(4,5)P_2, perhaps because the LAT cytoplasmic tail associated with PLC-γ1 can now access the plasma membrane or because PtdIns(4,5)P_2 is released from binding with the numerous actin binding/regulatory proteins it associates with[25, 26, 37, 45]. Alternatively, it has been shown that TCR stimulation results in PLC-γ1 translocation to the cortical actin cytoskeleton[46]. Actin turnover may therefore enhance PLC-γ1 recruitment to the membrane, and thus position it close to PtdIns(4,5)P_2. PtdIns(4,5)P_2 hydrolysis ensures further propagation of the proximal TCR signal to the calcium signaling and Ras-Erk signaling modules via the generation of the critical second messengers Ins(1,4,5)P_3 and DAG. We suggest that the role of the cortical actin cytoskeleton in regulating access of signaling enzymes to substrates may apply to other membrane receptor signaling pathways in other cell types.

Online Methods

Generation of Csk^{AS} mice

BAC RP24-400B5 containing the region of chromosome 9 with the *Csk* locus was from BACPAC Resources at the Children's Hospital Oakland Resource Institute. The following modifications were engineered by bacterial recombination-mediated genetic engineering[47]: 1-Mutation of the sequence encoding the mouse Csk threonine residue at position 266 to sequence encoding glycine. 2-Deletion on both ends of the BAC to leave Chr9: 57,602,462-57,676,881 (GRCm38.p1 C57BL/6J assembly). 3-Introduction of an in-frame stop codon in exon 2 of *Lman1L* gene. The modified BAC was injected into fertilized C57BL/6 embryos by the UCSF Transgenic and Targeted Mutagenesis Core Facility. Transgenic founders were crossed to *Csk*$^{-/-}$ mice[10]. Mice were genotyped with the following PCR primers: transgenic allele, 5′-AATAGGGAAGGGGGAGTTTG-3′ and 5′-CTTGGCCATGTACTCTCC-3′; wild-type allele, 5′-AATAGGGAAGGGGGAGTTTG −3′ and 5′-CTTGGCCATGTACTCTGT-3′

Mice

Mice used for these studies were 4–12 weeks of age. MHCI/MHCII deficient *H2-Ab1*$^{-/-}$ *B2m*$^{-/-}$ mice were from Taconic. *Icam1*$^{-/-}$ and *Cd80* $^{-/-}$ *Cd86*$^{-/-}$ mice were previously described[48, 49]. All mice were housed in a specific pathogen-free facility at UCSF according to the University Animal Care Committee and National Institutes of Health (NIH) guidelines.

Inhibitors

3-IB-PP1 has been described[20] and was used at 10 μM. Cytochalasin D, Latrunculin A and Jasplakinolide (Sigma) were used at 10 μM, 0.5 μM and 1 μM, respectively.

Antibodies and Reagents

CD3 PerCPCy5.5 (BD Biosciences, 551163), CD3 Alexa-647 (BD Biosciences 557869), CD4 PerCP-Cy5.5 (BD Biosciences 550954), CD4 PE (BD Biosciences 553730), CD5 FITC (BD Biosciences 553021), CD8 FITC and Alexa-647 (UCSF monoclonal antibodies core facility, clone YTS169.4), CD8 PECy7 (BD Biosciences 552877), CD11b PE (BD Biosciences 553311), CD11c PE (BD Biosciences 553802), CD19 PE (eBioscience

12-0193-83), CD25 PerCPCy5.5 (BD Biosciences 551071), CD44 FITC (BD Biosciences 553133), CD69 PECy7 (BD Biosciences 552879), CD90.2 APC (BD Biosciences 553007), B220 Alexa-647 (BD Biosciences 557683), γδ TCR PE (BD Biosciences 553178), NK1.1 PE (BD Biosciences 553165), Gr1 PE (BD Biosciences 553128), Siglec H Alexa-647 (Biolegend 129608); p44/42 MAPK pThr202/Tyr204 (4377), Src 416 (2101), ZAP-70-pY319 (2701), LAT (9166), pAkt-Ser473 (4058) are from Cell Signaling; LAT-pY132 (44–224), PLC-γ1-pY783(44–696G) and Phalloidin-Alexa 488 (A12379) are from Life Technologies; Csk (Santa Cruz C20); Phospho-tyrosine (Upstate 4G10); Phospho-tyrosine PY20, PLC-γ1 (05–163) are from Millipore; actin (Sigma Aldrich A2066); Lck (1F6 from J. B. Bolen); ζ (H146 from H. Wang); CD3ε (2C11), ZAP-70 (1E7.2) are from Harlan; Lck-pY505 (BD Biosciences 612390); Goat anti-armenian hamster IgG(H+L) (127-005-160) and donkey anti-rabbit IgG Ab conjugated to APC (711-136-152) are from Jackson Immunoresearch; Horseradish peroxidase (HRP)–conjugated goat antibody against rabbit IgG (H+L) (4050-05) and mouse IgG (H+L) (1031-50), rabbit anti-hamster IgG (H+L) (6215-05) are from Southern Biotech; B7.2 Ig (R&D Systems 741-B2-100).

Flow Cytometry and data analyses

Stained cells were analyzed on a BD Fortessa (BD Biosciences). Data analysis was performed using FlowJo software (Treestar Incorporated).

Statistical analyses

Statistical analyses with paired *t*-tests were performed using Microsoft Excel (Microsoft). Sample size choice and assumption of normality were based upon similar analyses from previously published studies.

Cell stimulations and intracellular phosphoflow

Before stimulations, cells were serum-starved at 37 °C for at least 15 min. Stimulations were performed in serum-free RPMI at 37 °C. CD3ε crosslinking was induced by addition of 20 μg/ml anti-CD3ε followed by goat anti-armenian hamster IgG(H+L) to a final concentration of 50 μg/ml. For bead-based stimulations, 4.5 μm styrene beads (Polyscience) were coated overnight with B7.2 Ig (5 μg/ml) and/or I-A^b tetramer loaded with human class II-associated invariant chain peptide 103–117 (5 μg/ml; NIH tetramer core facility) in PBS under continuous rotation at 4 °C. Beads were then saturated with 1% BSA PBS under continuous rotation for at least 1 h at 25 °C, and washed with PBS before use. Intracellular phospho-Erk and phospho-Akt staining was performed as previously described[20].

Calcium flux assays

Cells were loaded with the Indo1-AM (1.5μM, Invitrogen) for 30 min at 37 °C in RPMI with 5% fetal bovine serum, washed, surface stained and kept on ice in 5% FBS-RPMI. Cells were warmed to 37 °C for 5 min before stimulation.

Immunoblotting and Immunoprecipitation

Cells were lysed directly in 6x SDS-PAGE sample buffer after stimulation. Proteins were separated on SDS-PAGE gels, transferred to Immobilon-P polyvinylidene difluoride

membranes (Millipore) by standard immunoblotting techniques, and visualized with SuperSignal ECL reagent or SuperSignal West Femto maximum sensitivity substrate (Pierce Biotechnology) on a Kodak Imaging Station. For immunoprecipitations, cells were lysed in 1% NP-40 lysis buffer with protease and phosphatase inhibitors, and lysates were incubated overnight at 4 °C with protein G-sepharose beads preincubated with anti-ζ antibody. Immunoprecitates were washed with 3×1 ml lysis buffer before elution from beads.

Microscopy

Cell-bead conjugates were fixed in 4 % paraformaldehyde and 0.2% glutaraldehyde for 30 min at 25 °C. After spin-washes in PBS and staining buffer (PBS with 2% FCS), cells are permeabilized in 0.05% Triton X-100 for 5 min and washed with staining buffer. After 30 min in staining buffer, conjugates were stained with CD90.2-APC (BD Biosciences) and phalloidin-Alexa488 (Life technologies). *z*-stacks of conjugates were imaged unmounted in Ibidi 96 well plates with 40x air objective on Zeiss Axiovert 200M. Best focus of cell-bead interface was scored for polarized F-actin towards bead, while stimulus identity was blinded.

Cell enrichments

Enriched populations of $CD4^+$ T cells or pan T cells were obtained by negative selection according to manufacturer's protocol (STEMCELL Technologies, 19752, 19751). Enriched populations of DCs were obtained by CD11c-positive selection according to manufacturer's protocol (STEMCELL Technologies, 18758 or 18780). Thymic DCs were obtained by grinding thymi in gentleMACS C tubes (Miltenyi Biotec) with Spleen 2 program, digesting at 37 °C. for 20 min with 62.4 μg/ml DNaseI (Roche) and 1.25 mg/ml collagenase D (Worthington), then further grinding with the Spleen 1 program. The single cell suspension obtained was surface stained and then sorted for $CD11^c$ positive cells after dumping B220, CD3, Siglec H and side scatter high cells.

Total inositol phosphates measurement

Thymocytes (4×10^7 cells/ml) were labeled with 40 μCi/ml of [^{3}H]-myo-inositol (Perkin Elmer) for 6 h at 37 °C, washed and cultured overnight at 37 °C in complete RPMI. Labeled thymocytes were treated with 20 mM lithium chloride for 20 min at 37 °C and stimulated as appropriate. Cells were lysed in 0.75 ml of chloroform-methanol-12M hydrochloric acid (100:200:2) and the phases were separated by the addition of 0.25 ml H_2O and 0.25 ml chloroform. The upper aqueous phase was mixed with 2.3 ml H_2O and the precipitate formed pelleted. The aqueous phase was then applied to columns made from 1.2 ml of a 0.5 g/ml aqueous slurry of AG 1-X8 (Biorad 140–1444). [^{3}H]-Inositol and [^{3}H]-glycerophosphorylinositol were washed off with 18 ml of 60 mM sodium formate–5 mM disodium tetraborate solution. Total inositol phosphates were eluted with 10 ml of 1 M ammonium formate plus 0.1 M formic acid. Radioactivity was determined by scintillation counting in Ecoscint (National Diagnostics).

Protein Purification

cDNAs encoding full-length mouse Csk (Csk^{WT}), the PP1-analog-sensitive mutant T266G (Csk^{AS}), and the kinase-impaired mutant K222R ($Csk^{K222R,50}$) were subcloned into a

pGEX-6P-3 vector containing an N-terminal glutathione S-transferase (GST) affinity tag. Each vector was transformed into BL21(DE3) cells (Agilent), and expression was induced with 0.2 mM isopropyl-β-D-thio-galactoside (IPTG) at 18 °C overnight. The bacterial pellet was resuspended in GST binding buffer, pH 7.4 (phosphate-buffered saline (PBS) with 5 mM EDTA and 5 mM dithiothreitol (DTT)) and lysed by freeze/thaw, lysozyme treatment, and sonication (Branson 450). All purification steps were performed on ice or at 4 °C, and all columns and proteases were obtained from GE Healthcare. Clarified lysate was affinity purified by binding to a GST Gravitrap column and elution at pH 8.0 with 10 mM reduced glutathione, 25 mM Tris, 50 mM NaCl, and 1 mM DTT. The GST tag was cleaved with PreScission Protease overnight. After buffer exchange by concentration and dilution, Csk was further purified by HiTrap Q anion exchange chromatography at pH 8.0 (50 mM Tris, 50 – 1000 mM NaCl, and 1 mM DTT) followed by a Superdex 200 gel filtration column in 100 mM NaCl, 10% Glycerol, and 50 mM Tris, pH 8.0. Purified Csk was flash frozen in liquid nitrogen and stored at −70°C. Homogeneity and molecular weight of purified proteins were verified by SDS PAGE and mass spectrometry. The concentration of purified Csk was determined from its absorbance at 280 nm using a molar absorptivity of 73800 M^{-1} cm^{-1} calculated by ExPASy ProtParam[51].

Kinase Activity Assays

The activity of purified Csk was obtained from a continuous spectrometric assay in which ATP hydrolysis is coupled via pyruvate kinase and lactate dehydrogenase to NADH oxidation, which results in a decrease in absorbance at 340 nm[52]. Kinase activity was measured at 30 °C with a Molecular Devices Spectramax 340PC spectrophotometer in a 75 μl reaction volume with final concentrations of 2.5 μM Csk, 55.7 U/ml pyruvate kinase, 78 U/ml lactate dehydrogenase, 0.6 mg/ml NADH, 1 mM phosphoenolpyruvate, 250 μM ATP, 10 mM Tris pH 7.5, 1 mM $MgCl_2$, and 1 mM tris(2-carboxyethyl)phosphine (TCEP). The reaction was initiated by adding a final concentration of 250 μM Csk optimal peptide substrate (KKKKEEIYFFF,[53]) synthesized by Elim Biosciences. Negligible background activity was observed if substrate or kinase was omitted from the reaction. Kinase activity was obtained by fitting the initial segment of the decay curve to a linear function. Reported data represent four separate experiments. For IC_{50} curves, independent samples were mixed with DMSO containing varying concentrations of 3-IB-PP1 just prior to the initiation of the reaction. Linear velocities were obtained at each concentration of 3-IB-PP1 and normalized between 0 and 100% within each data set. Five independent data sets with Csk^{AS} and four with Csk^{WT} were fit globally to the function $y = 100/(1+10\text{^}((x\text{-}\log IC_{50})))$ to determine the IC_{50} value. All curve fitting and statistical analysis was performed using Graphpad Prism.

Supplementary Material

Refer to Web version on PubMed Central for supplementary material.

Acknowledgements

We thank A. Roque and Z. Wang for assisting with animal husbandry and cell sorting, respectively. We thank N. Killeen and Z. Yang for technical assistance with BAC transgenesis, J.S. Shin for technical assistance with isolation of thymic DCs and H. Liu and the UCSF Helen Diller Family Comprehensive Cancer Center Mass Spectrometry Core Facility for technical and analytical expertise. We thank J.A. Bluestone for providing CD80-CD86 deficient

mice. We thank J. Bolen and H. Wang for providing Lck and CD3 ζ antibodies respectively. We thank A. DeFranco, C. Lowell and H. Wang for critical reading of the manuscript and helpful discussions. Y.X.T. is funded by the Agency for Science, Technology and Research in Singapore. B.N.M. is funded by the Cancer Research Institute Irvington Postdoctoral Fellowship. This work was supported in part by NIH grants PO1 AI091580 (A.W.) and 5R01EB001987 (K.M.S).

References

1. Smith-Garvin JE, Koretzky GA, Jordan MS. T cell activation. Annu Rev Immunol. 2009; 27:591–619. [PubMed: 19132916]
2. van Oers NS, Killeen N, Weiss A. ZAP-70 is constitutively associated with tyrosine-phosphorylated TCR zeta in murine thymocytes and lymph node T cells. Immunity. 1994; 1:675–685. [PubMed: 7600293]
3. Xu C, et al. Regulation of T cell receptor activation by dynamic membrane binding of the CD3epsilon cytoplasmic tyrosine-based motif. Cell. 2008; 135:702–713. [PubMed: 19013279]
4. James JR, Vale RD. Biophysical mechanism of T-cell receptor triggering in a reconstituted system. Nature. 2012; 487:64–69. [PubMed: 22763440]
5. van der Merwe PA, Dushek O. Mechanisms for T cell receptor triggering. Nat Rev Immunol. 2011; 11:47–55. [PubMed: 21127503]
6. Palacios EH, Weiss A. Function of the Src-family kinases, Lck and Fyn, in T-cell development and activation. Oncogene. 2004; 23:7990–8000. [PubMed: 15489916]
7. Bergman M, et al. The human p50csk tyrosine kinase phosphorylates p56lck at Tyr-505 and down regulates its catalytic activity. Embo J. 1992; 11:2919–2924. [PubMed: 1639064]
8. Hermiston ML, Xu Z, Majeti R, Weiss A. Reciprocal regulation of lymphocyte activation by tyrosine kinases and phosphatases. J Clin Invest. 2002; 109:9–14. [PubMed: 11781344]
9. Nika K, et al. Constitutively active Lck kinase in T cells drives antigen receptor signal transduction. Immunity. 2010; 32:766–777. [PubMed: 20541955]
10. Imamoto A, Soriano P. Disruption of the csk gene, encoding a negative regulator of Src family tyrosine kinases, leads to neural tube defects and embryonic lethality in mice. Cell. 1993; 73:1117–1124. [PubMed: 7685657]
11. Nada S, et al. Constitutive activation of Src family kinases in mouse embryos that lack Csk. Cell. 1993; 73:1125–1135. [PubMed: 8513497]
12. Schmedt C, et al. Csk controls antigen receptor-mediated development and selection of T-lineage cells. Nature. 1998; 394:901–904. [PubMed: 9732874]
13. Cloutier JF, Chow LM, Veillette A. Requirement of the SH3 and SH2 domains for the inhibitory function of tyrosine protein kinase p50csk in T lymphocytes. Mol Cell Biol. 1995; 15:5937–5944. [PubMed: 7565746]
14. Brdicka T, et al. Phosphoprotein associated with glycosphingolipid-enriched microdomains (PAG), a novel ubiquitously expressed transmembrane adaptor protein, binds the protein tyrosine kinase csk and is involved in regulation of T cell activation. J Exp Med. 2000; 191:1591–1604. [PubMed: 10790433]
15. Davidson D, Bakinowski M, Thomas ML, Horejsi V, Veillette A. Phosphorylation-dependent regulation of T-cell activation by PAG/Cbp, a lipid raft-associated transmembrane adaptor. Mol Cell Biol. 2003; 23:2017–2028. [PubMed: 12612075]
16. Kawabuchi M, et al. Transmembrane phosphoprotein Cbp regulates the activities of Src-family tyrosine kinases. Nature. 2000; 404:999–1003. [PubMed: 10801129]
17. Xavier R, Brennan T, Li Q, McCormack C, Seed B. Membrane compartmentation is required for efficient T cell activation. Immunity. 1998; 8:723–732. [PubMed: 9655486]
18. Dobenecker MW, Schmedt C, Okada M, Tarakhovsky A. The ubiquitously expressed Csk adaptor protein Cbp is dispensable for embryogenesis and T-cell development and function. Mol Cell Biol. 2005; 25:10533–10542. [PubMed: 16287865]
19. Xu S, Huo J, Tan JE, Lam KP. Cbp deficiency alters Csk localization in lipid rafts but does not affect T-cell development. Mol Cell Biol. 2005; 25:8486–8495. [PubMed: 16166631]

20. Schoenborn JR, Tan YX, Zhang C, Shokat KM, Weiss A. Feedback circuits monitor and adjust basal Lck-dependent events in T cell receptor signaling. Sci Signal. 2011; 4:ra59. [PubMed: 21917715]
21. Gamper CJ, Powell JD. All PI3Kinase signaling is not mTOR: dissecting mTOR-dependent and independent signaling pathways in T cells. Front Immunol. 2012; 3:312. [PubMed: 23087689]
22. Berridge MJ. Inositol trisphosphate and calcium signalling mechanisms. Biochim Biophys Acta. 2009; 1793:933–940. [PubMed: 19010359]
23. Kortum RL, et al. A phospholipase C-gamma1-independent, RasGRP1-ERK-dependent pathway drives lymphoproliferative disease in linker for activation of T cells-Y136F mutant mice. J Immunol. 2013; 190:147–158. [PubMed: 23209318]
24. Kusumi A, et al. Paradigm shift of the plasma membrane concept from the two-dimensional continuum fluid to the partitioned fluid: high-speed single-molecule tracking of membrane molecules. Annu Rev Biophys Biomol Struct. 2005; 34:351–378. [PubMed: 15869394]
25. Blin G, et al. Quantitative analysis of the binding of ezrin to large unilamellar vesicles containing phosphatidylinositol 4,5 bisphosphate. Biophys J. 2008; 94:1021–1033. [PubMed: 17827228]
26. Gambhir A, et al. Electrostatic sequestration of PIP2 on phospholipid membranes by basic/aromatic regions of proteins. Biophys J. 2004; 86:2188–2207. [PubMed: 15041659]
27. Treanor B, et al. The membrane skeleton controls diffusion dynamics and signaling through the B cell receptor. Immunity. 2010; 32:187–199. [PubMed: 20171124]
28. Klein L, Hinterberger M, Wirnsberger G, Kyewski B. Antigen presentation in the thymus for positive selection and central tolerance induction. Nat Rev Immunol. 2009; 9:833–844. [PubMed: 19935803]
29. Proietto AI, Lahoud MH, Wu L. Distinct functional capacities of mouse thymic and splenic dendritic cell populations. Immunol Cell Biol. 2008; 86:700–708. [PubMed: 18779841]
30. Burkhardt JK, Carrizosa E, Shaffer MH. The actin cytoskeleton in T cell activation. Annu Rev Immunol. 2008; 26:233–259. [PubMed: 18304005]
31. Veillette A, Bookman MA, Horak EM, Bolen JB. The CD4 and CD8 T cell surface antigens are associated with the internal membrane tyrosine-protein kinase p56lck. Cell. 1988; 55:301–308. [PubMed: 3262426]
32. Steinman RM. Decisions about dendritic cells: past, present, and future. Annu Rev Immunol. 2012; 30:1–22. [PubMed: 22136168]
33. Boomer JS, Green JM. An enigmatic tail of CD28 signaling. Cold Spring Harb Perspect Biol. 2010; 2:a002436. [PubMed: 20534709]
34. Salazar-Fontana LI, Barr V, Samelson LE, Bierer BE. CD28 engagement promotes actin polymerization through the activation of the small Rho GTPase Cdc42 in human T cells. J Immunol. 2003; 171:2225–2232. [PubMed: 12928366]
35. Liang Y, et al. The lymphoid lineage-specific actin-uncapping protein Rltpr is essential for costimulation via CD28 and the development of regulatory T cells. Nat Immunol. 2013; 14:858–866. [PubMed: 23793062]
36. Abraham RT, Weiss A. Jurkat T cells and development of the T-cell receptor signalling paradigm. Nat Rev Immunol. 2004; 4:301–308. [PubMed: 15057788]
37. Saarikangas J, Zhao H, Lappalainen P. Regulation of the actin cytoskeleton-plasma membrane interplay by phosphoinositides. Physiol Rev. 90:259–289. [PubMed: 20086078]
38. Valitutti S, Dessing M, Aktories K, Gallati H, Lanzavecchia A. Sustained signaling leading to T cell activation results from prolonged T cell receptor occupancy. Role of T cell actin cytoskeleton. J Exp Med. 1995; 181:577–584. [PubMed: 7836913]
39. Kraus M, Alimzhanov MB, Rajewsky N, Rajewsky K. Survival of resting mature B lymphocytes depends on BCR signaling via the Igalpha/beta heterodimer. Cell. 2004; 117:787–800. [PubMed: 15186779]
40. Polic B, Kunkel D, Scheffold A, Rajewsky K. How alpha beta T cells deal with induced TCR alpha ablation. Proc Natl Acad Sci U S A. 2001; 98:8744–8749. [PubMed: 11447257]
41. Gross JA, Callas E, Allison JP. Identification and distribution of the costimulatory receptor CD28 in the mouse. J Immunol. 1992; 149:380–388. [PubMed: 1320641]

42. Buhlmann JE, Elkin SK, Sharpe AH. A role for the B7-1/B7-2:CD28/CTLA-4 pathway during negative selection. J Immunol. 2003; 170:5421–5428. [PubMed: 12759417]
43. Dautigny N, Le Campion A, Lucas B. Timing and casting for actors of thymic negative selection. J Immunol. 1999; 162:1294–1302. [PubMed: 9973382]
44. Holdorf AD, et al. Proline residues in CD28 and the Src homology (SH)3 domain of Lck are required for T cell costimulation. J Exp Med. 1999; 190:375–384. [PubMed: 10430626]
45. van Rheenen J, et al. EGF-induced PIP2 hydrolysis releases and activates cofilin locally in carcinoma cells. J Cell Biol. 2007; 179:1247–1259. [PubMed: 18086920]
46. Patsoukis N, et al. RIAM regulates the cytoskeletal distribution and activation of PLC-gamma1 in T cells. Sci Signal. 2009; 2:ra79. [PubMed: 19952372]
47. Tischer BK, von Einem J, Kaufer B, Osterrieder N. Two-step red-mediated recombination for versatile high-efficiency markerless DNA manipulation in Escherichia coli. Biotechniques. 2006; 40:191–197. [PubMed: 16526409]
48. Sligh JE Jr. et al. Inflammatory and immune responses are impaired in mice deficient in intercellular adhesion molecule 1. Proc Natl Acad Sci U S A. 1993; 90:8529–8533. [PubMed: 8104338]
49. Borriello F, et al. B7-1 and B7-2 have overlapping, critical roles in immunoglobulin class switching and germinal center formation. Immunity. 1997; 6:303–313. [PubMed: 9075931]
50. Chow LM, Fournel M, Davidson D, Veillette A. Negative regulation of T-cell receptor signalling by tyrosine protein kinase p50csk. Nature. 1993; 365:156–160. [PubMed: 8371758]
51. Gasteiger, E., et al. Protein Identification and Analysis Tools on the ExPASy Server. Walker, John M., editor. The Proteomics Protocols Handbook, Humana Press; 2005.
52. Barker SC, et al. Characterization of pp60c-src tyrosine kinase activities using a continuous assay: autoactivation of the enzyme is an intermolecular autophosphorylation process. Biochemistry. 1995; 34:14843–14851. [PubMed: 7578094]
53. Sondhi D, Xu W, Songyang Z, Eck MJ, Cole PA. Peptide and protein phosphorylation by protein tyrosine kinase Csk: insights into specificity and mechanism. Biochemistry. 1998; 37:165–172. [PubMed: 9425036]

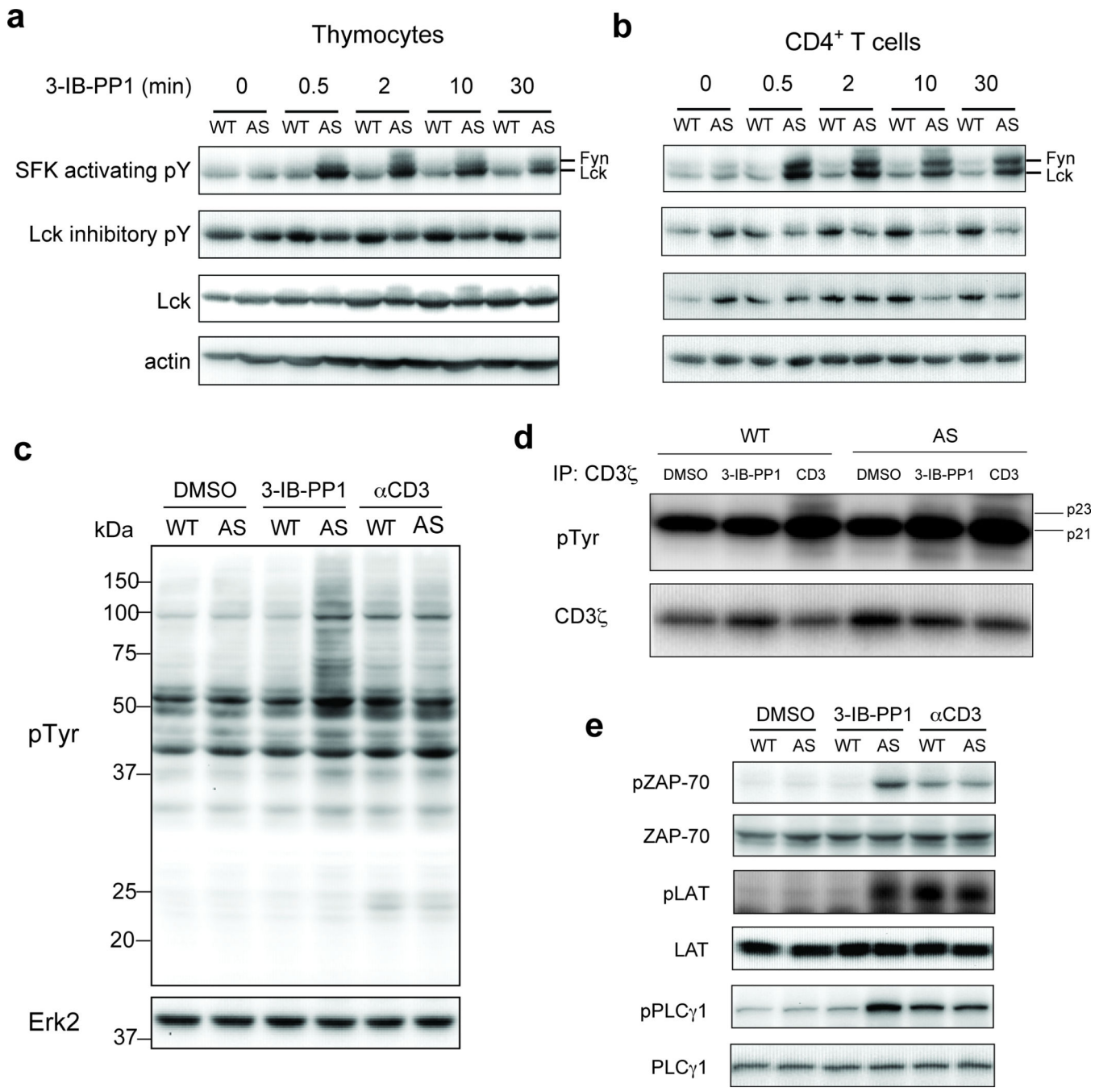

Figure 1.

Inhibition of Csk^{AS} in primary murine T cells induces hyperactivation of SFKs and phosphorylation of TCR proximal signaling molecules. (**a**) Wild-type (WT) or Csk^{AS} (AS) thymocytes or (**b**) peripheral $CD4^+$ T cells were treated for the indicated times with 10 μM 3-IB-PP1 and analyzed by immunoblotting. (**c**) Wild-type (WT) or Csk^{AS} (AS) thymocytes were treated for 3 min with vehicle (DMSO), 3-IB-PP1 or anti-CD3ε and analyzed by immunoblotting. (**d**) Wild-type (WT) or Csk^{AS} (AS) thymocytes were treated for 3 min with vehicle (DMSO), 10μM 3-IB-PP1 or 20μg/mL anti-CD3ε, then lysed and

immunoprecipitated with anti-CD3 ζ antibody. Immunoprecipitates were analyzed by immunoblotting. (**e**) Wild-type (WT) or Csk^{AS} (AS) thymocytes were treated for 3 min with vehicle (DMSO), 10μM 3-IB-PP1 or 20μg/mL anti-CD3ε and analyzed by immunoblotting. All data are representative of 3 independent experiments.

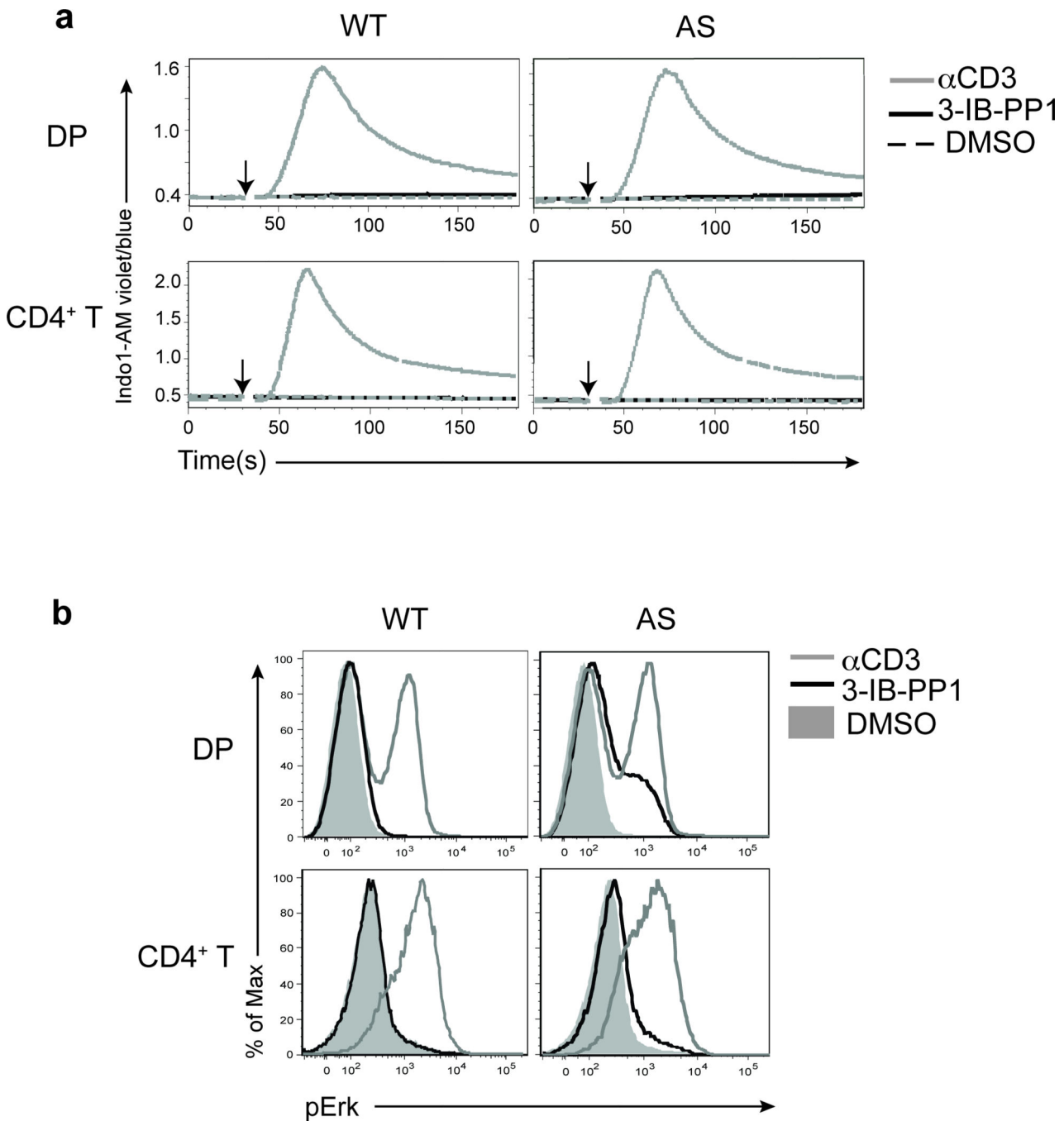

Figure 2.

Increases in intracellular calcium and Erk phosphorylation are impaired following Csk^{AS} inhibition. (**a**) Wild-type (WT) or Csk^{AS} (AS) thymocytes or purified peripheral $CD4^+$ T cells loaded with Indo-1AM dye were stimulated with vehicle (DMSO: shaded gray histogram), 10μM 3-IB-PP1 (black) or 20μg/mL anti-CD3ε (gray). Ratiometric assessment of intracellular calcium of $CD4^+CD8^+$ thymocytes or $CD4^+$ T cells over time is shown. (**b**) Wild-type (WT) or Csk^{AS} (AS) thymocytes or splenocytes were stimulated for 2 min with vehicle (DMSO: shaded gray histogram), 10μM 3-IB-PP1 (black) or 20μg/mL anti-CD3ε

(gray), then analyzed for pErk content. Histograms are gated on $CD4^+CD8^+$ thymocytes or $CD4^+$ splenocytes. All data are representative of three independent experiments.

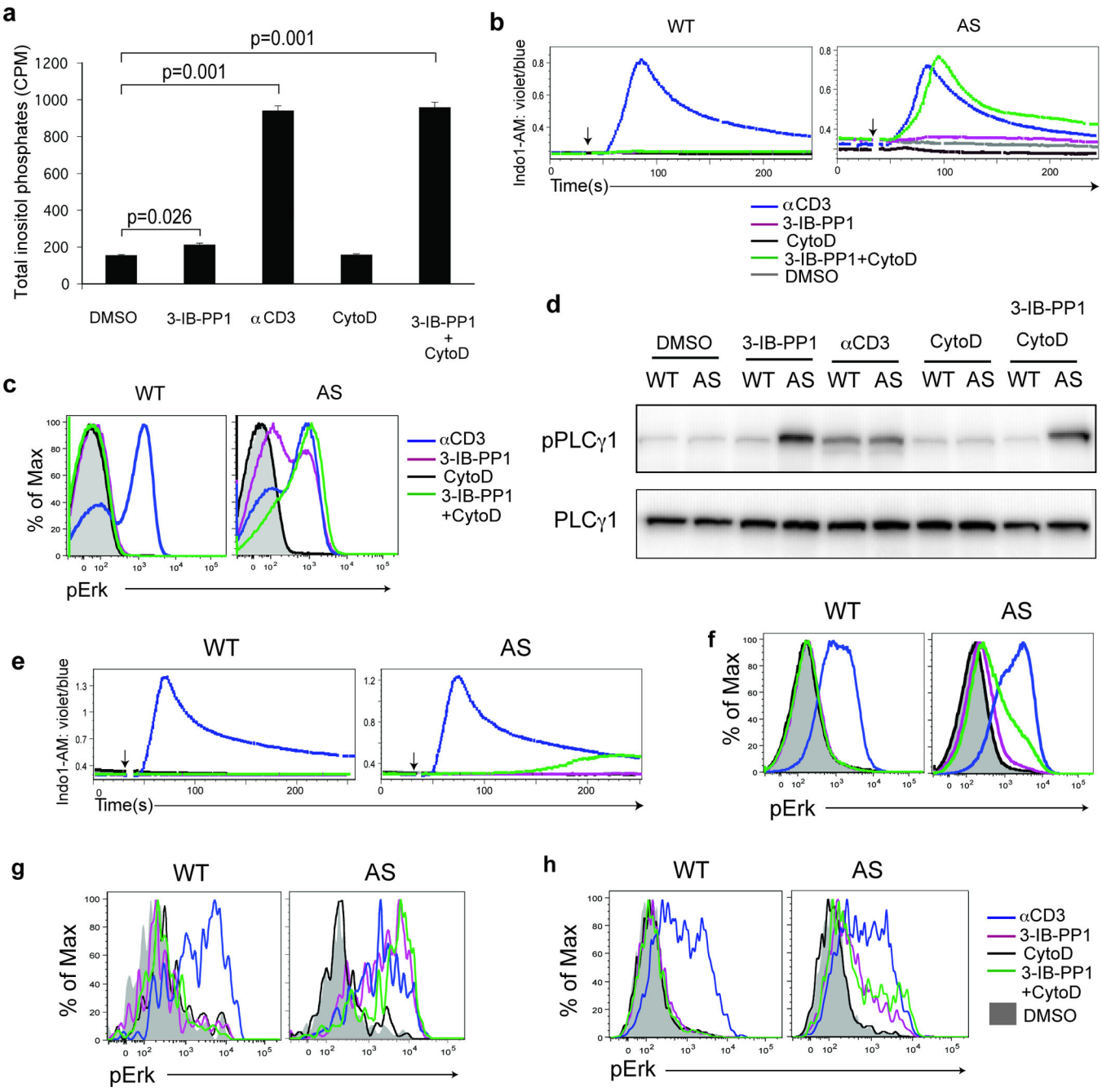

Figure 3.

Calcium flux and Erk phosphorylation are restored by altering the actin cytoskeleton following Csk^{AS} inhibition. (**a**) Csk^{AS}(AS) thymocytes were stimulated with vehicle (DMSO), 10μM 3-IB-PP1, 20μg/mL anti-CD3ε, 10μM cytochalasin D (CytoD) alone or with 10μM 3-IB-PP1 for 5 min, and total inositol phosphate content was measured (mean, ± S.E.M., $n = 3$ (technical replicates), *P*-values from paired two-tailed student's *t*-test). (**b**) Wild-type (WT) or Csk^{AS} (AS) thymocytes were stimulated with vehicle (DMSO: gray), 10μM 3-IB-PP1 (magenta), 20μg/mL anti-CD3ε (blue), 10μM cytochalasin D (CytoD: black) alone or with 10μM 3-IB-PP1(green). Ratiometric assessment of intracellular calcium

of $CD4^+CD8^+$ thymocytes over time is shown. (**c**) Wild-type (WT) or Csk^{AS} (AS) thymocytes were stimulated for 2 min as in **b**, then analyzed for pErk content. Histograms are gated on $CD4^+CD8^+$ thymocytes. (**d**) Wild-type (WT) or Csk^{AS} (AS) thymocytes were treated for 3 min as in **a** and analyzed by immunoblotting. (**e**) Wild-type (WT) or Csk^{AS} (AS) splenocytes were stimulated as in **b**. Ratiometric assessment of intracellular calcium of CD4+ splenocytes over time is shown. (**f**) Wild-type (WT) or Csk^{AS} (AS) splenocytes were stimulated for 2 min as in **b**, then analyzed for pErk content. Histograms are gated on $CD4^+$ splenocytes. Shaded histogram is DMSO control. (**g**) Wild-type (WT) or Csk^{AS} (AS) thymocytes or (**h**) purified T cells were stimulated for 2 min as in **b**, then analyzed for pErk content. Histograms are gated on $CD4^-$ $CD8^-$ γδ TCR^+ cells.. All data are representative of three independent experiments.

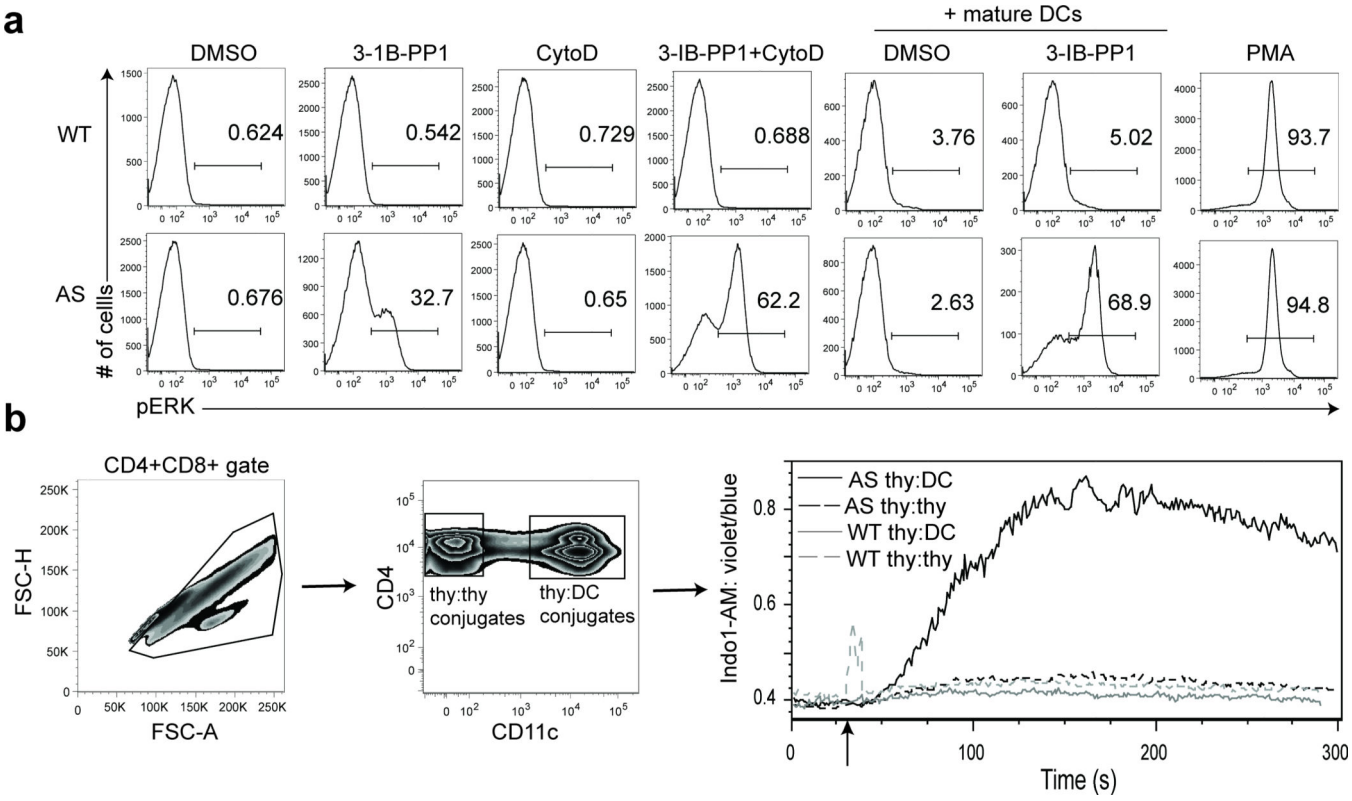

Figure 4.

Mature DCs restore calcium flux and Erk phosphorylation following Csk^{AS} inhibition. (**a**) DCs enriched from wild-type splenocytes were activated by overnight culture. Thymocytes from wild-type (WT) or Csk^{AS}(AS) mice were pelleted with or without activated DCs at a 1:1 ratio and stimulated with vehicle (DMSO), 10μM 3-IB-PP1, 10μM cytochalasin D (CytoD) alone or with 10μM 3-IB-PP1 or 50ng/mL phorbol myristate acetate (PMA) for 3 min. Cells were then analyzed for pErk content. Histograms shown are gated on $CD4^+CD8^+$ thymocytes. Numbers within histograms indicate percentage of $pErk^+$ cells. (**b**) Wild-type (WT) or Csk^{AS} (AS) thymocytes were loaded with Indo1-AM dye and surface stained for CD4 and CD8. Activated DCs were prepared as in **a**, and surface stained for CD11c. Thymocytes and activated DCs were mixed at a 1:1 ratio and stimulated for 5 min with 10μM 3-IB-PP1. Cells collected were first gated for $CD4^+CD8^+$ multiplets, then further separated into thymocyte-thymocyte conjugates ($CD11c^-$) and thymocyte-DC conjugates ($CD11c^+$) before ratiometric assessment of intracellular calcium over time (far right). All data are representative of three independent experiments.

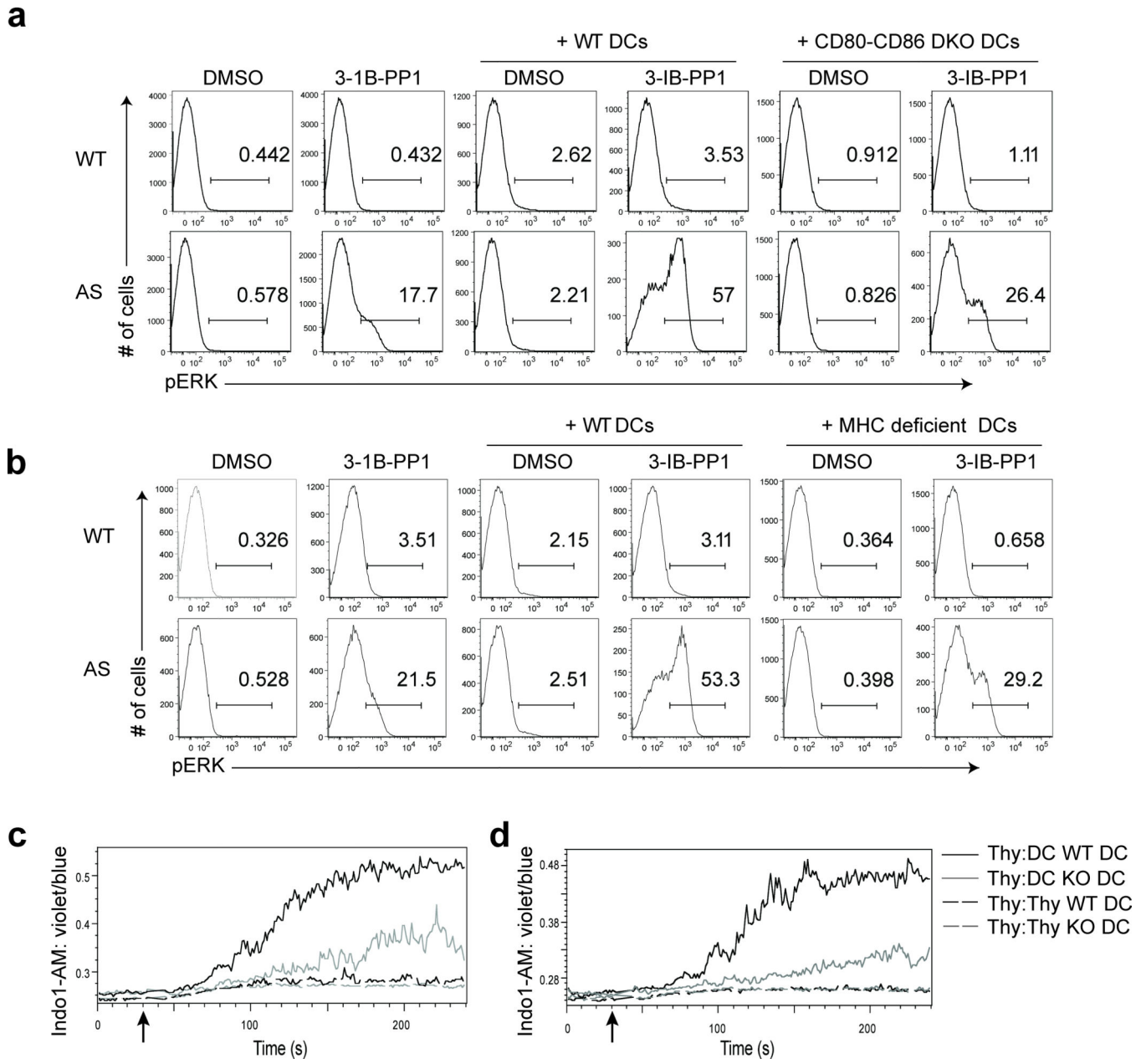

Figure 5.

Restoration of full TCR signaling upon Csk^{AS} inhibition requires both MHC and B7 on DCs. DCs enriched from wild-type or (**a**) CD80-CD86 double knockout or (**b**) MHCI and MHCII deficient splenocytes were activated by overnight culture. Wild-type (WT) or Csk^{AS} (AS) thymocytes were pelleted with or without activated DCs at a 1:1 ratio and stimulated with vehicle (DMSO) or 10μM 3-IB-PP1for 3 min. Cells were then analyzed for pErk content. Histograms shown are gated on $CD4^{+}CD8^{+}$ thymocytes. Numbers within histograms indicate percentage of $pErk^{+}$ cells. (**c, d**) Wild-type (WT) or Csk^{AS} (AS) thymocytes were loaded with Indo1-AM dye and surface stained for CD4 and CD8. Activated DCs from (**c**) CD80-CD86 double knockout or (**d**) MHCI- and MHCII-deficient splenocytes were surface stained for CD11c. Thymocytes and activated DCs were mixed at

a 1:1 ratio and stimulated with 10μM 3-IB-PP1. Cells collected were first gated for $CD4^+CD8^+$ multiplets, then further separated into thymocyte-thymocyte conjugates ($CD11c^-$) and thymocyte-DC conjugates ($CD11c^+$) before ratiometric assessment of intracellular calcium over time. All data are representative of three independent experiments.

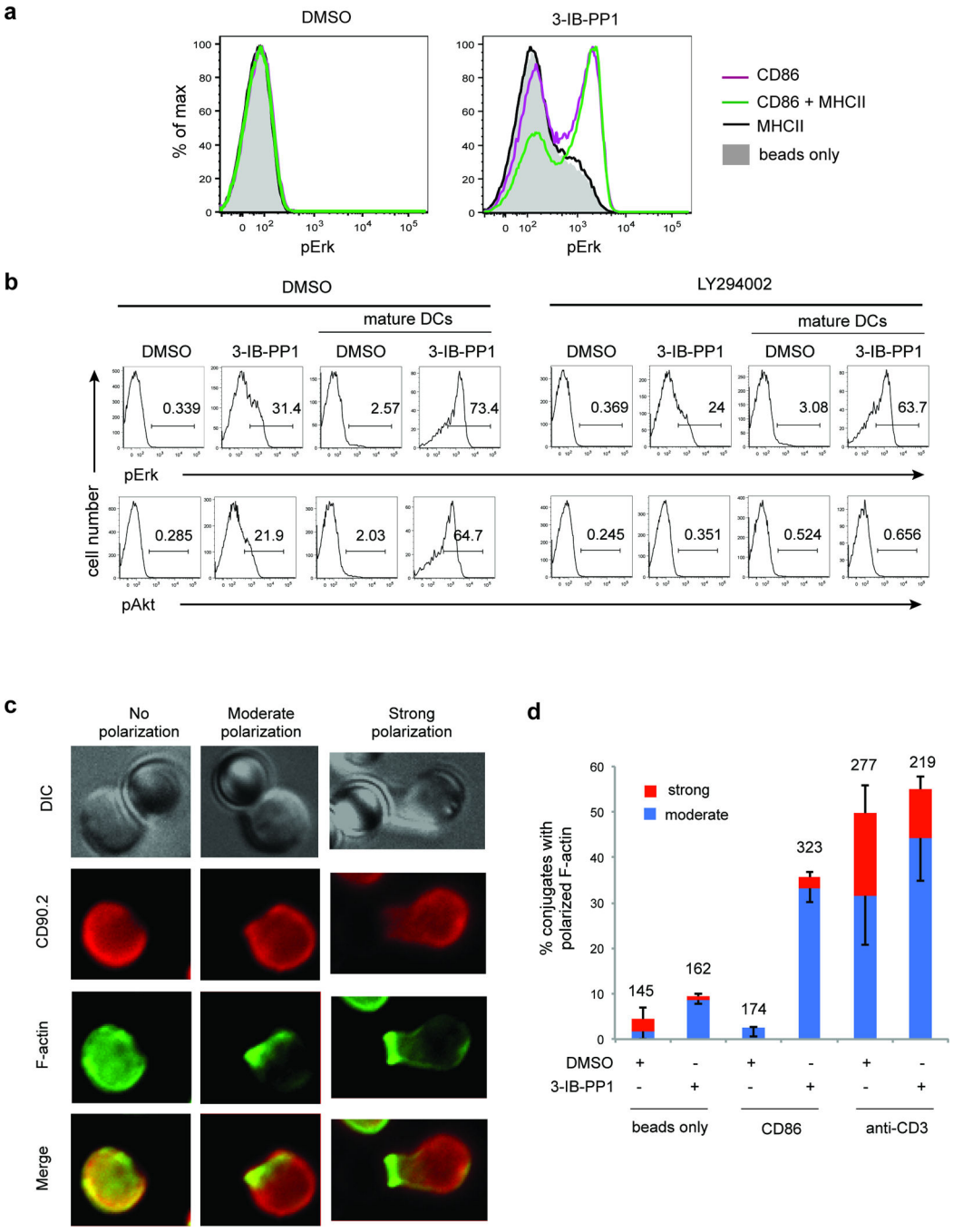

Figure 6.

CD28 signaling induces actin remodeling and restores robust Erk phosphorylation following Csk^{AS} inhibition. (**a**) Csk^{AS} thymocytes were pelleted with styrene beads coated with 5 μg/ml CD86-Ig (CD86) and/or 5 μg/ml I-A^b tetramer (MHCII) and treated for 3 min with vehicle (DMSO) or 10 μM 3-IB-PP1 and then analyzed for pErk content. Histograms shown are gated on $CD4^+CD8^+$ thymocytes. Data shown are representative of three independent experiments. (**b**) Csk^{AS} thymocytes were pretreated for 15 min with DMSO or 10 μM LY294002, then pelleted with or without activated WT DCs at a 1:1 ratio and stimulated as

indicated for 3 min. Cells were then analyzed for pErk and pAkt content. Histograms shown are gated on $CD4^+CD8^+$ thymocytes. Numbers within histograms indicate percentage of $pErk^+$ or $pAkt^+$ cells. Data shown are representative of three independent experiments. (**c, d**) Csk^{AS} thymocytes were pelleted with styrene beads coated with 5 μg/ml CD86-Ig or 5 μg/ml anti-CD3ε and treated for 3 min with vehicle (DMSO) or 10μM 3-IB-PP1. Bead-thymocyte conjugates were imaged for F-actin distribution. (**c**) Representative images show the different F-actin distribution patterns observed. (**d**) Graph shows the percentage of conjugates with moderate and strong F-actin polarization at the bead-thymocyte interface (means, -S.E.M.(moderate), +S.E.M.(strong), $n = 3$ (biological replicates)). Total number of conjugates analyzed for each condition is indicated on top of the bars.